ON-CHIP MONITORING OF MEMS GEAR MOTION

Danelle M. Tanner, Scot E. Swanson, Jeremy A. Walraven, and Jeffrey L. Dohner
Sandia National Laboratories, P.O. Box 5800, MS 1081, Albuquerque, NM 87185-1081
Web page: http://www.mems.sandia.gov email: tannerdm@sandia.gov

ABSTRACT

We have designed and fabricated a polysilicon sidewall-contact motion monitor that fits in between the teeth of a MEMS gear. The monitor has a center grounded member that is moved into contact with a pad held at voltage. We have succeeded in observing motion, however, the monitor fails after only a few actuations. A thorough investigation of the contacting interfaces revealed that for voltages > 5 V with a current limit of 100 μA, the main conduction process is Fowler-Nordheim tunneling. After a few switch cycles, the polysilicon interfaces became insulating. This is shown to be a permanent change and the suspected mechanism is field-induced oxidation of the asperity contacts. To reduce the effects of field-induced oxidation, tests were performed at 0.5 V and no permanent insulating case was observed. However, the position of the two contacting surfaces produced three types of conduction processes a) Fowler-Nordheim tunneling, b) ohmic, and c) insulator, which were observed in a random order during switch cycling. The alignment of contact asperities produced this positional effect.

INTRODUCTION

A sensor or monitor that can be seamlessly integrated into any design would enable long-term reliability testing of MEMS (Micro-ElectroMechanical System). This monitor should contribute a minimal load on the actuator, should be built on-chip, and should provide electrical signals for ease of information gathering. Simplicity in the electrical technique would allow implementation on large-scale experiments. Most MEMS inspection techniques rely on optical methods [1], which constrain the type and breadth of reliability experiment that can be performed. This paper documents the development of an on-chip method to electrically monitor the motion of gears. This method can be applied to all in-plane motion.

Although using an optical interface is quite manageable when characterizing a device with available interferometric techniques [2, 3], it severely limits the ability to perform the suite of experiments needed to fully test the device reliability. MEMS devices in hermetically sealed packages need expensive sapphire windows to detect motion. Temperature, shock, and vibration stress tests have to be performed unactuated, and then checked after the test. In addition, many of the qualification tests, such as aging, require storage for long periods of time in controlled environments. Removing the device for periodic testing disrupts the environment and has the potential to introduce additional failure modes. A self-contained, on-chip electrical monitor will allow data acquisition in all of these cases.

MONITOR DESIGNS

We have fabricated two different types of monitors; one was a cantilever design and the other a torsional spring design. Both use the same general feature of a flexible member placed between the teeth of a gear. The monitors are designed in a polysilicon laminate layer with a thickness of 2.5 μm and roughly 10-ohms/squaresheet resistances. As the gear turns, the center member gets displaced and contacts a pad held at voltage. Charge will flow as a result of this contact. If we connect a power supply in constant current mode, we can sense the abrupt change in voltage as the charge starts to flow.

We chose a monitor design that used DC electrical techniques as the simplest, easiest to implement approach. An alternate method would use capacitive sensing. The capacitance of this design is on the order of tens of femptofarads and would be difficult to measure without on-chip amplification, not available with the SUMMiT™ technology.

The cantilever design is shown in the Scanning Electron Microscope images (SEM) of Figure 1 with a close-up view of the placement in the gear teeth shown in the lower-right inset. Contact pads, held at voltage, on both sides of the flexible center member allow for detection of clockwise (V_{cw}) or counter clockwise (V_{ccw}) motion of the gear. The contact pad dimensions shown in the inset are 5 μm long and 2.5 μm deep yielding a 12.5-μm^2 contact area. The beams are 1 μm wide in the as-fabricated position and the contact pads are separated by 2 μm. We fabricated three lengths, 50, 75, and 100 μm. The light contrast of the V_{cw} was due to charging from the electron

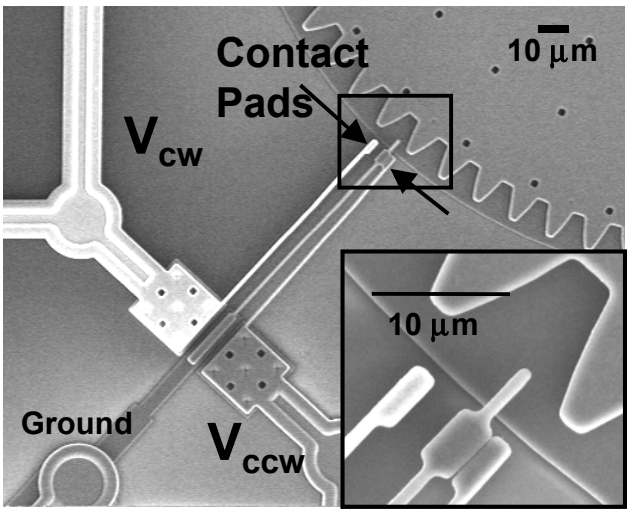

Figure 1. This cantilever beam design SEM image shows the structure and a magnified view of its placement in the gear tooth region in the lower-right inset. The switch is in contact mode due to charging by the electron beam.

beam. The flexible center member and the moving gear are grounded. Note that in the inset, it appears that V_{ccw} shorted to the grounded center member. Electrostatic forces induced by the electron beam pulled the polysilicon components together.

The torsional spring design is shown in Figure 2 with a close-up view of the placement in the gear teeth shown in the lower-right inset. We can also monitor both directions using this design. There were two variations in the stiffness of the spiral springs and 3 variations in the contact pad stiffness. The change in stiffness of the spiral spring was achieved by fabricating a mechanical clamp in the spiral as shown in Figure 3. The three variations of contact pad stiffness were achieved by the addition of serpentine springs as shown in Figure 4. All of the spiral spring designs required more total force than the cantilever designs, which was a large load for our two types of actuators, microengines and TRAs (Torsional Ratcheting Actuator).

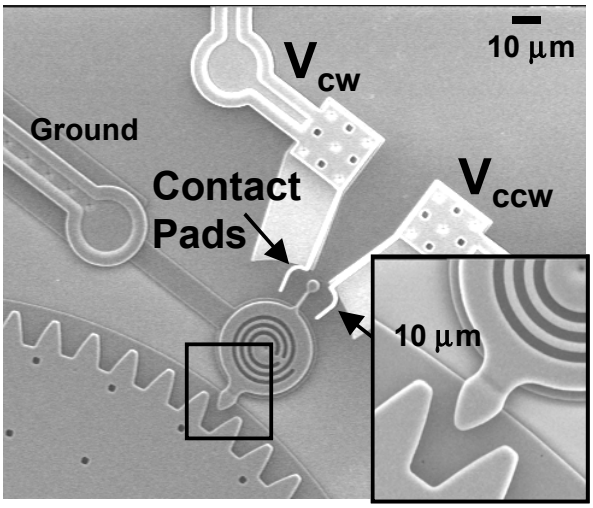

Figure 2. This torsional switch design image shows the structure and a magnified view of its placement in the gear tooth region in the lower-right inset.

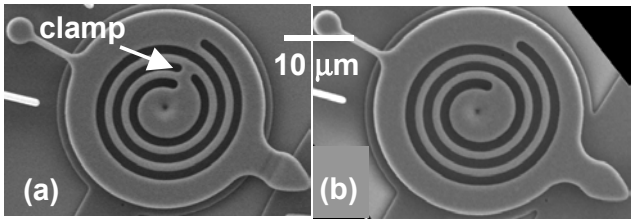

Figure 3. Spiral spring with (a) and without (b) the mechanical clamp.

Monitor designs were modeled and results were visualized using the pre and post processing code PATRAN™ and models were simulated using the non-linear processing code ABAQUS.™ Represented physics included quasi-static mechanics and frictionless contact. Simulations were performed to determine the force required to operate each switch. This force was the maximum reaction force between the gear and its contact location. This force occurred just prior to gear/switch separation. Gear teeth were modeled and an enforced displacement was applied. This approximated the movement of a rack (or a gear of very large radius) passing through the switch. Contact was invoked between the gear and the switch (load force) and between locations internal to the switch (contact force). These internal contact locations were used to shunt or open the flow of current to an

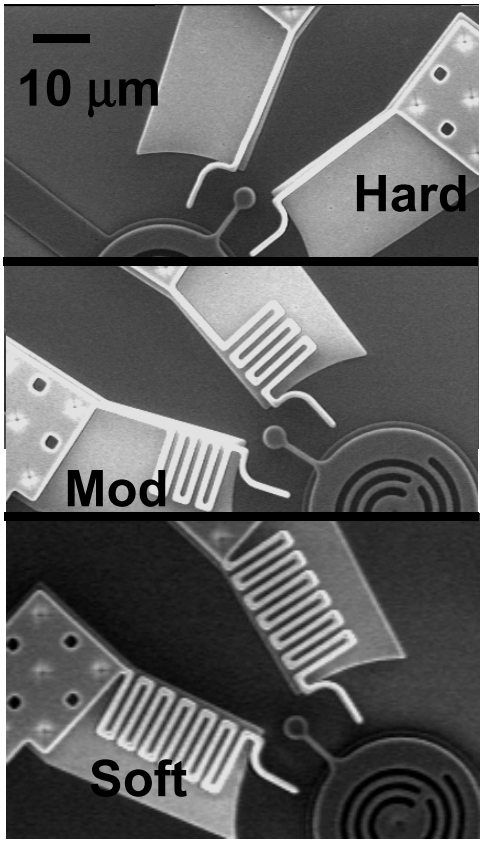

Figure 4. Views of the hard, moderate, and soft contact pads.

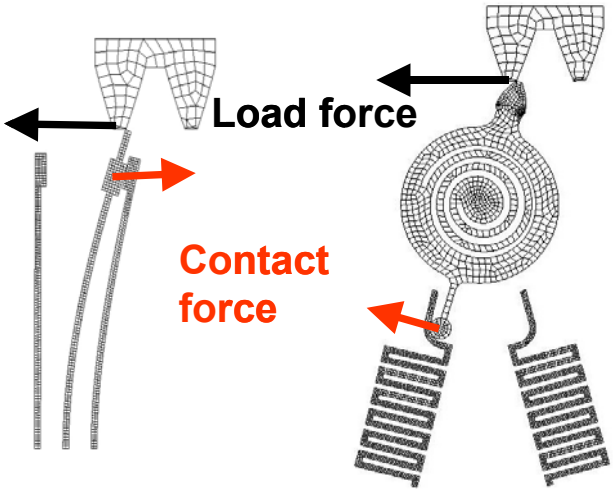

Figure 5. Visualization of models for both types of monitors.

attached circuit. Graphical representations of both types of switches are shown in Figure 5.

Nine monitor designs were analyzed – three beam switches and six torsional switches. The analysis results can be found in Table 1. The beam switches were 50, 75, and 100 µm in length and required forces of 12.8, 4.6 and 2.3 µN, respectively. The contact forces between the center beam and the outer beam were roughly half of the beam load forces. Torsional switches were constructed from a helical spring that could be mechanically clamped at a location along its length to vary the stiffness. Unclamped switches required a load force

of 10μN to operate, whereas, clamped switched required a load force of about 16μN.

Table 1. Predicted load force and contact force for the monitor designs.

Monitor Designs	Load Force (μN)	Contact Force (μN)
50 μm Beam	12.8	6.6
75 μm Beam	4.6	2.2
100 μm Beam	2.3	1.1
Clamped Torsion		
Soft	16	0.1
Medium	16	0.25
Hard	16	0.3
Unclamped Torsion		
Soft	10	0.1
Medium	10	0.25
Hard	10	0.3

Internal to the monitor were contact locations. The reaction forces between contacting locations were monitored by tracking nodal forces. For the 50, 75, and 100 μm beam switches the contact forces were 6.6, 2.2, and 1.1 μN. For the torsion switches, the contact force was a strong function of the contacting spring stiffness. The softest springs produced contact loads of about 0.1 μN, the moderate springs produced contact loads of about 0.25 μN, and the hardest springs produced contact loads of about 0.3 μN.

Experimental Methods

Constant Current: In the experiments using an actuator to move the gear and the monitor, we used a constant-current data acquisition method. An HP4156 in sampling mode, was configured with SMU (Source Measurement Unit) current source with 20V compliance through the closed switch.. In this case, an open switch would appear as 20 V and a closed switch would measure a few volts.

Voltage Sweep: In experiments where we wanted to investigate the closed switch interface, we used an HP4156 to sweep a voltage across the closed switch and monitored the current. We determined that a current of 1 mA would fuse the switch readily, thus we maintained a current compliance of 100 μA in all tests.

Current Time Profile: There were a few cases where we held a constant voltage on a closed switch and measured the current over time. These tests were performed using an HP4156 in sampling mode with 100-μA compliance.

Experimental Results

Initial results from both the cantilever and torsional design are shown in Figure 6. The plots show the gear tooth motion of a TRA running at 10 Hz. Each was triggered manually during TRA operation. A voltage reading of 20 V implies an open condition and near 0 V implies a closed condition. There is some periodicity in the monitor signal, but also erratic contact. We observed irregular motion of the TRA ring during the measurement, which probably contributed to the erratic contact. Additionally, the TRA has some radial wobble [4]

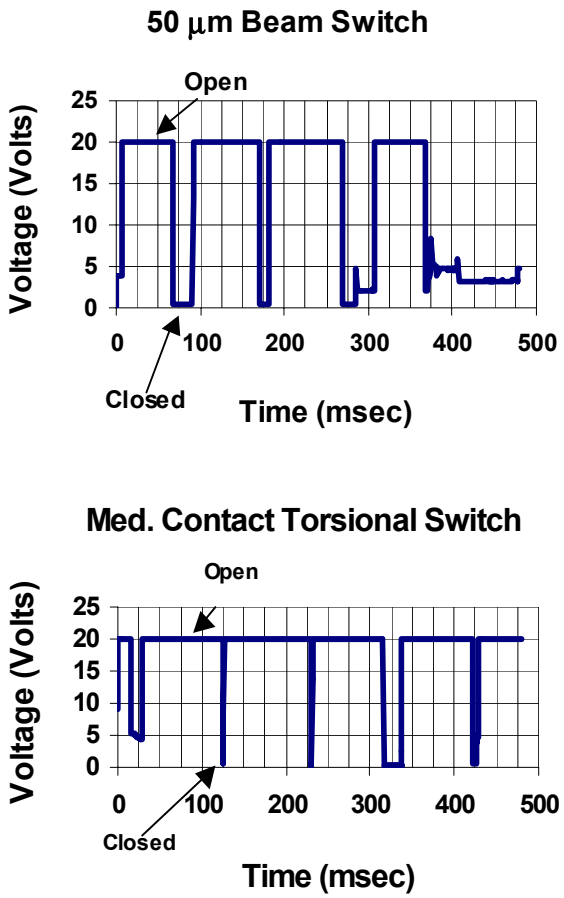

Figure 6. Manual-triggered monitor signals showing the motion of the ring gear of a TRA at a 10 Hz drive frequency. The upper graph shows the signal from the 50 μm cantilever beam switch with 12.8 μN of load force and the lower graph shows the signal from the torsional switch with roughly 18 μN of load force.

that contributed to the switch contact. Future designs will link the TRA to a larger gear, which should eliminate the wobble.

In the SUMMiT™ process, all sidewall materials are polycrystalline silicon giving rise to large contact resistance that varies according to the force on the contact pad. We circumvented this contact resistance issue by monitoring the voltage change of a constant-current power supply. The designs with the higher contact force requirements worked best, probably because of the increased contact pressure. However, these designs also subject the actuator to the high loads, which is not conducive to seamless implementation of the monitor.

The major problem found with the switch devices was that after some small number of contacts (5-10), the closed switch becomes insulating. The next section documents our work in investigating the interface contacts of the monitor.

Monitor Interface Investigation

We performed voltage sweeps of closed monitors and measured the current through the interface. The monitors were closed manually with a probe tip in all cases. These experiments took place in ambi-

ent laboratory environment, which ranged from 20 to 22 °C and 20 to 40 %RH. All of the following experiments were performed on the 75-µm long cantilever beam monitor as shown in Figure 1. This monitor has more contact area than the torsional design and overall gave more consistent results. The contact area was 2.5 µm thick by 5-µm long, yielding a potential contact area of 12.5 μm^2. This contact area was formed between the sidewalls of two polysilicon structures. We assumed that a native oxide (2-3 nm) existed on both surfaces.

In the first case, we held the switch closed (static switch test) and then swept the voltage 10 successive times while monitoring the current. The current compliance was set to 100 µA and the peak sweep voltage was 20V. A typical Fowler-Nordheim I-V curve was observed, as shown in Figure 7. Note that the first sweep was erratic, but all following sweeps were very consistent.

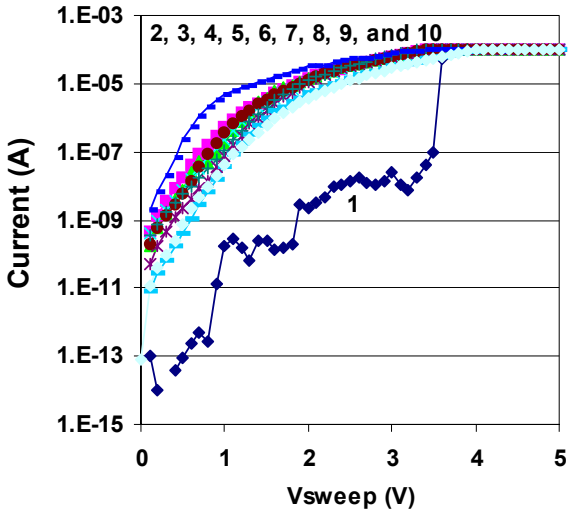

Figure 7. Current versus voltage curve for a static switch. The switch was held closed and 10 successive voltage sweeps to 20 V were recorded. Each sweep is labeled.

In order to investigate the effect of switching, we opened and closed the switch manually after each voltage sweep. We found that hot switching, where the voltage is held on one leg of the monitor during actuation, and cold switching, where the voltage was removed, produced similar results. In both cases, the switch interface becomes insulating after a small number of sweeps. Figure 8 shows the current-voltage plots for both cases. The sweep number is indicated on the plot.

For the case of the hot switching in Figure 8, repeated switches after sweep 8 revealed the same insulating behavior. Ten additional sweeps were performed with no change in the current-voltage data. We conclude from this that the damage/change was permanent for this 20V sweep.

For the case of cold switching in Figure 8, note the intermediate data for sweeps 7 and 9. This behavior was occasionally noticed during hot switching also. Both of these cases eventually reached compliance.

Failure analysis of these failed contact surfaces was performed to better understand why the switches became insulating. SEM examination of the contacting interface revealed several key features of the

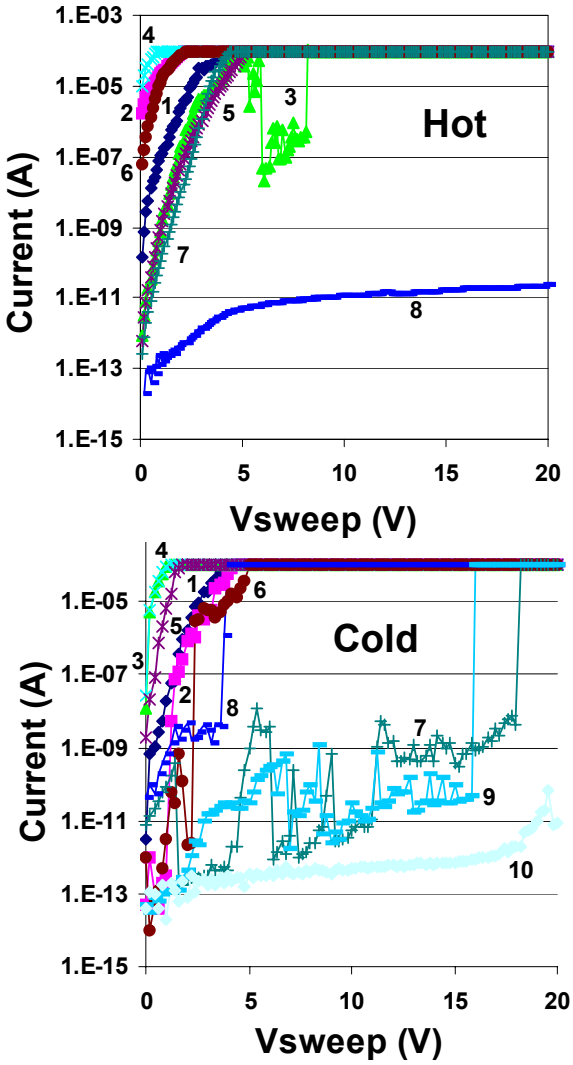

Figure 8. Current versus voltage plots for hot and cold-switched experiments. Note that for the hot-switched case, and insulating interface was created after only 7 switches. For the cold-switched case, an insulating interface was created after 9 switches. Each sweep is labeled.

switching mechanism. Figure 9a shows the initial contact region of the device. In normal operation, more of the surface area will contact (see model in Figure 5). This initial contact site is compared to a reference switch shown in Figure 9b. In Figure 9b, note the shape of the polysilicon sidewalls in the as-fabricated state. No processing, surface damage, or contamination was observed along the reference surfaces.

Understanding the contact mechanism provides insight into analyzing the region of the switch where contact is first made. Examination of an electrical switch that failed after 8 switching cycles (became insulating) revealed some surface damage along the same region where initial contact was made. This is shown in Figure 10. The damage site is consistent with the contact site shown in Figure 9a. Transmission Electron Microscopy (TEM) analysis of the vertical sidewalls (contact interface) was attempted to gain insight into the deformation and oxidation along those edges but was inconclusive.

Although TEM analysis was not successful, the failure mechanism leading to insulation over a limited number of contact cycles

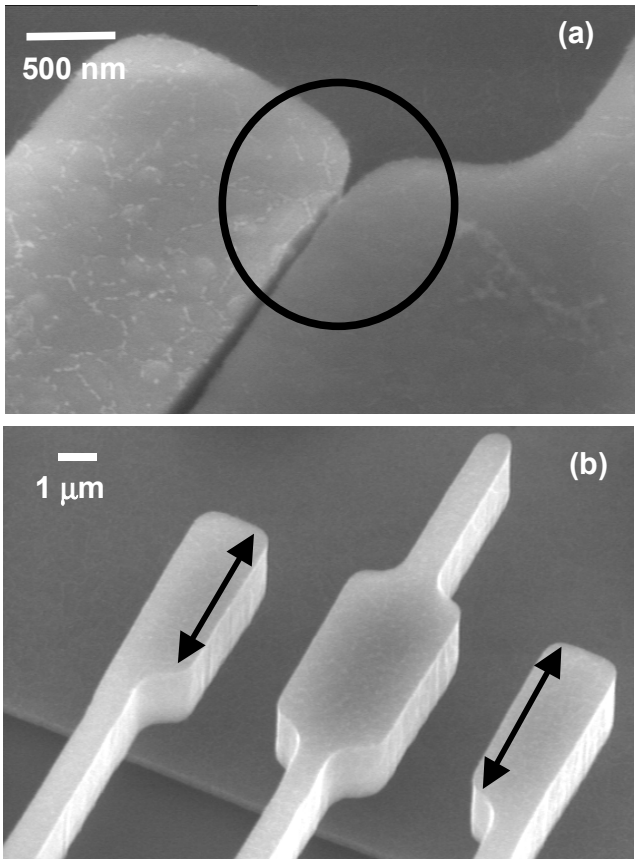

Figure 9a and b. a) Contact switch electrostatically pulled into contact with the grounded central component reveals only a small contact site along the top most edge. b) Open switch showing the entire contact surfaces indicated by the arrows.

may be due to field-induced oxide growth at the interface. This oxidation process was observed using scanning tunneling microscopy (STM) over a silicon surface in air. [5, 6] The typical threshold reported for this process is 10^9 V/m which is quite achievable in our switch closure, assuming we have 20 V across 4 nm of native oxide ($5x10^9$ V/m). Additionally, any surface roughness with asperities would enhance this effect by producing more oxide along the contacting asperities.

To minimize any field-induced oxide growth, we changed the peak sweep voltage to 0.5 V. This allowed probing of the interface very early in the voltage sweep giving a snapshot of the current behavior. Using the same hot-switching technique employed earlier, we observed the data in Figure 11. The individual sweeps are labeled in the plot. The data naturally group into three sets named A, B, or C. The sweeps appear to be randomly distributed across the three interfaces. We suspect that this may be a positioning effect depending on how the surface asperities matched up. In each of these switch actuations, the surfaces appear to be in contact visually. Note that at this lower voltage, we observe **no** permanent change to the surfaces.

By analyzing the I-V data for groups A and B, we can determine the voltage dependence and identify the type of conduction process as defined in Sze. [7] Group A data were fit with a tunnel or field emission model (Fowler – Nordheim) where the current dependence is proportional to $-V^2\exp(-b/V)$. The current data from group B fit equally well with a V or V^2 dependence. The V dependence would be simple ohmic conduction and the V^2 indicates a space-charge-

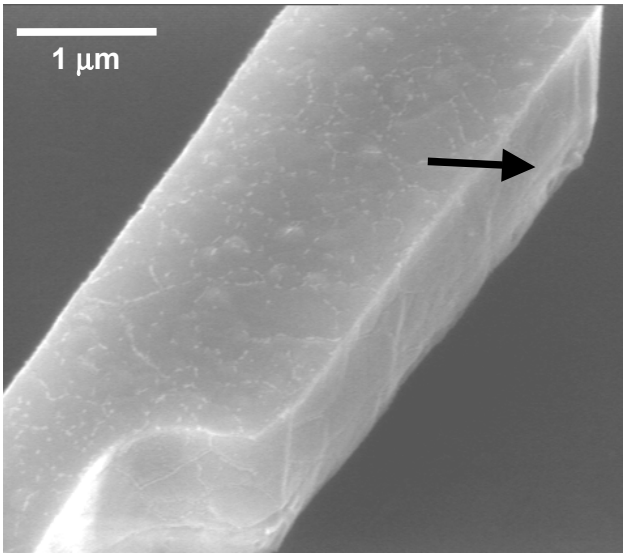

Figure 10. Damage site (arrow) identified along the lower edge of the electrical switch that failed after 8 switching cycles.

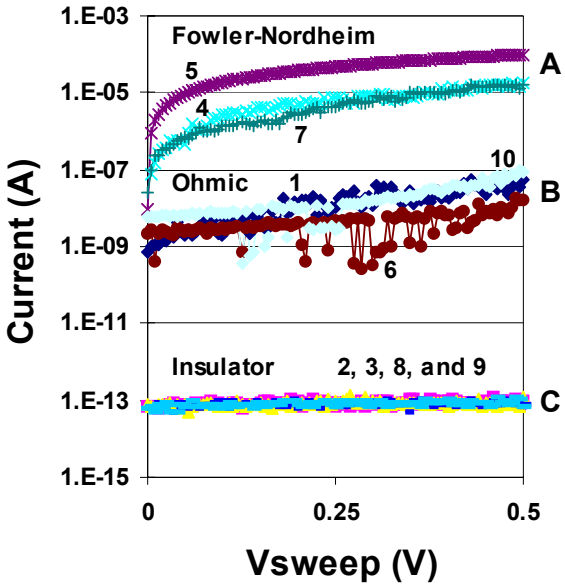

Figure 11. Current versus voltage plots for hot-switched experiments at a reduced voltage of 0.5 V showing like data grouped as A, B, or C. Each group corresponds to a different conduction process labeled on the graph.

limited conduction process. Group C appeared perfectly insulating, with current data at the lower limit of our measurement capability.

At these small scales, any current conduction between the sidewall surfaces most likely was through the asperities. We were unable to acquire a sidewall surface roughness measurement. The sidewall roughness is defined during etch of the sacrificial oxide and a slight pattern of vertical lines was observed in Figures 9 and 10. Our hypothesis with positioning is that when tunneling was observed, the hills and valleys of the two surfaces mated well (small gap) producing high current flow. The other extreme where we see no current flow (large gap) could be asperity hill-on-hill alignment with native oxide on the surfaces. The ohmic contact could then be something in between with a more random alignment.

Looking more closely at the 0.5 V case, we performed cold switch experiments where the voltage was held constant and we observed the current over time for a period of 100 seconds. As shown in Figure 12, in three out of five cases, the current remains constant. However, in two cases, the current is decreasing and then between 20 to 30 seconds it drops by 3 to 8 orders of magnitude (sweeps 4 and 5). This same pattern was observed in a single test where 5 V was applied which put the meter into 100-μA compliance limit. At roughly 23 seconds, the current dropped to 40 nA. We are not sure what caused this effect at 20 seconds.

In the next series of tests, we doubled the peak voltage in steps to try to gain understanding of the grown insulating layer. The results are shown in Figure 13. The initial 5-volt sweep was hot switched until an insulating layer was grown (sweep 4). Three 10-volt sweeps were attempted, but were unsuccessful at breaking down the insulating layer. An increase in voltage to 20 volts broke through the insulating layer (sweeps 8 and 9), but created another insulator during sweep 10. Increasing to 40 volts breaks down the insulating material, and in subsequent sweeps, darkened the polysilicon contact until the final sweep (16) fused the monitor.

Investigation of the monitor used in the voltage doubling experiment revealed that at 40 V, the failure mechanism was welding of the switching components to each other. The failed monitor shown in Figure 14a and b shows a molten region along the interface of the two contact surfaces. Given the data provided from this experiment, the failure mode(s) are; a) monitors become insulating after multiple exposures at lower voltages, b) monitors fuse to each other at higher voltages.

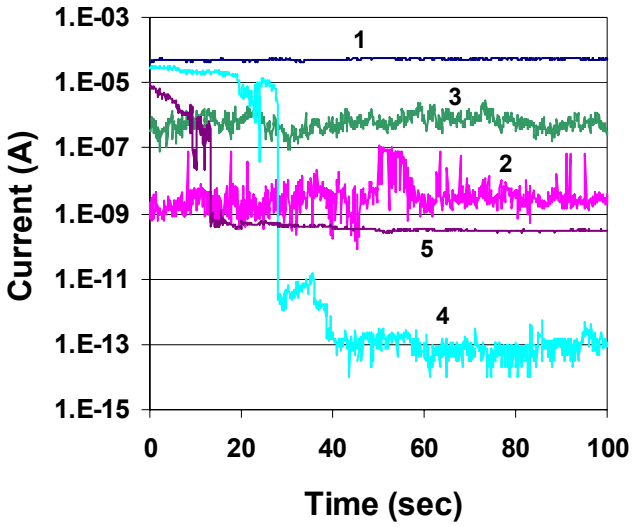

Figure 12. Current versus time for a cold-switched cantilever beam device held at 0.5 V.

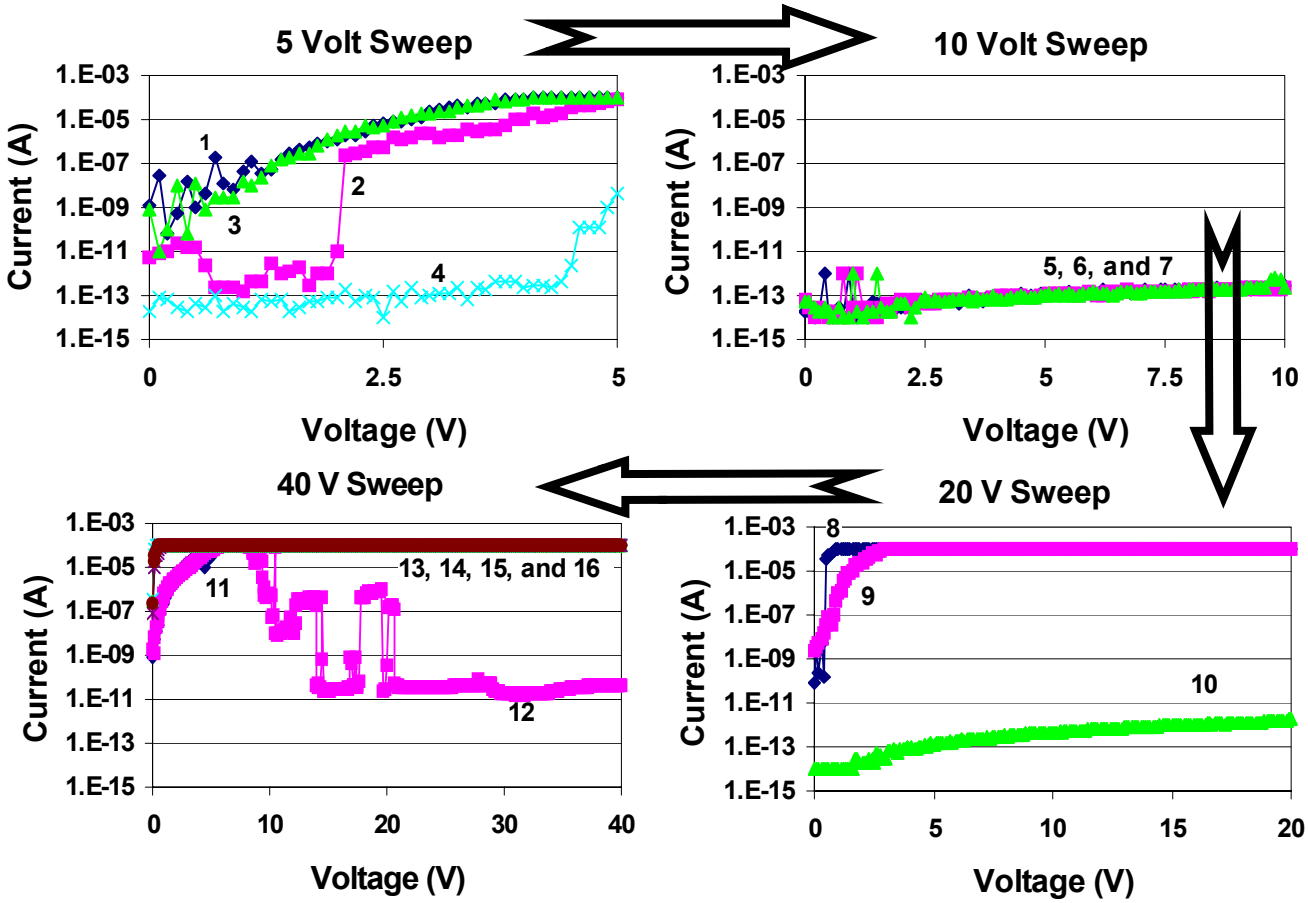

Figure 13. Current versus Voltage sweeps using a current compliance of 100 μA and a peak voltage as indicated on the plot.

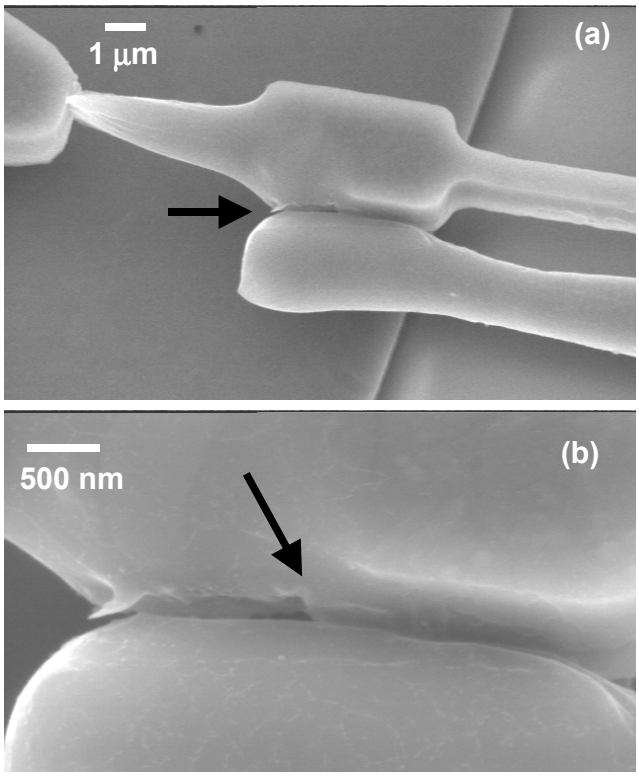

Figure 14a and b. Deformed and shorted monitor was the result of a voltage doubling experiment with a final sweep voltage of 40 V and 100 μA current compliance.

The failure mechanism described in a) is due to poor electrical contact attributed to positional effects of the monitor and/or a combination of positional affects with oxidation of contacting asperities. In this failure mode, the contacting surfaces begin passing current for a few cycles, then (while still in contact), no current passes through the monitor until the voltage is increased. Because the contact surfaces are smaller than the calculated 12.5-μm^2 areas, asperity-to-asperity contact plays a vital role in passing current. Here, the asperities that were in contact have probably been oxidized after switching cycles. With each increasing voltage step, the asperities oxidize until a critical oxide thickness is reached where current no longer flows. No signs of debris or the introduction of foreign material, etc. were found in the contact surfaces. After a few switching cycles, deformation is observed along the contacting portion of the switch, after the switch has become insulating.

The failure mechanism described in b) occurs when the maximum voltage to enhance the field-induced oxidation process broke through the oxide. Here, the voltage was high enough to allow the monitor to work for a few switching cycles. After the final switching cycle, the device fails in a stuck mode and is permanently shorted. This failure indicates the oxide layer has broken down by excessive heating of the contacting asperities and the polysilicon surfaces have fused together.

CONCLUSIONS

It has been shown that monitoring MEMS gear motion using these polysilicon switch designs is possible for a small number of actuations, but the monitor (run at 100 μA compliance) eventually becomes an insulator. The probable mechanism for insulator growth is field-induced oxidation at the tips of the mating surface asperities where the field is enhanced. This insulating effect was observed in both hot and cold-switched monitors. For peak sweep voltages > 5 volts, we consistently created a permanent insulating layer. Increasing the voltage temporarily restored functionality, but became insulating again. There was no debris or contamination observed on the contacting surfaces.

For peak sweep voltage of 0.5 volts, there was no indication of a permanent insulating layer. However, there were indications of positional dependence of the cantilever beam switches. We have observed an equal probability of actuation resulting in an insulator, an ohmic contact, or a tunneling layer with no sequential dependence. Visually the mechanical monitor appears closed in the same position for each actuation.

Although we'd like to use polysilicon contact surfaces because of minimal post-processing steps, this data indicates a need to preclude field-induced oxidation effects, possibly by metalizing the surfaces.

ACKNOWLEDGMENTS

We acknowledge the help of Sita Mani and the Microelectronics Development Lab for fabrication and the release of the structures used in this experiment. We thank Robert Fleming and Jim Allen who reviewed the paper. We also thank Fred Sexton for his support and guidance. Sandia is a multiprogram laboratory operated by Sandia Corporation, a Lockheed Martin Company, for the United States Department of Energy under contract DE-AC04-94-AL85000.

REFERENCES

[1] F. M. Dickey, S. C. Holswade, L. A. Hornak, K. S. Brown, "Optical methods for micromachine monitoring and feedback," in *Sensors and Actuators*, **78** (1999), pp. 220-235.

[2] W. Hemmert, M. S. Mermelstein, D. M.Freeman, "Nanometer resolution of three-dimensional motions using video interference microscopy," in *12th International Workshop on Micro Electro Mechanical Systems - MEMS, 17-21 Jan. 1999, Orlando, FL* p.302-8.

[3] D. J. Burns and H. F. Helbig, "A System for Automatic Electrical and Optical Characterization of Microelectromechanical Devices," *JMEMS*, **8**, No. 4, 1999, pp. 473-482.

[4] Danelle M. Tanner, Jeremy A. Walraven, Stephen M. Barnes, Norman F. Smith, Fernando Bitsie, and Scot E. Swanson, "Reliability of a MEMS Torsional Ratcheting Actuator," in *Proceedings of IRPS*, 2001, pp. 81-90.

[5] D. Stievenard, P. A. Fontaine, and E. Dubois, "Nanooxidation using a scanning probe microscope: An analytical model based on field induced oxidation," Appl. Phys. Lett. **70** (24), 16 June 1997, pp.3272-3274.

[6] J. A. Dagata, T. Inoue, J. Itoh, and H. Yokoyama, "Understanding scanned probe oxidation of silicon," in *Applied Physics Letters*, 1998, **73**, No. 2, pp. 271-273

[7] S. M. Sze, *Physics of Semiconductor Devices*, New York: John Wiley & Sons, 1981, p. 403.